A gravity-current model for the OWEL WEC — literature review and feasibility study —

by Hamid Alemi Ardakani

Department of Mathematics, University of Surrey, Guildford, Surrey GU2 7XH, England

Abstract. The OWEL wave energy converter is a floating rectangular device open at one end to capture the incoming wave field. The trapped waves in the duct hit the upper rigid lid and create a seal resulting in a moving trapped pocket of air ahead of the wave front which drives the power take off. Understanding the dynamics of the two phase flow created by the wave input is key to the energy optimisation of the power take off. A photo of a model OWEL vessel is shown below at the point where the wave has been trapped and begins to drive the pocket of air along the vessel with air takeoff at the upper right edge. The interior two-phase flow field in OWEL is very similar to a gravity-current configuration. The purpose of this document is to review gravity current theory and propose a theoretical and experimental strategy for adapting and modifying existing gravity current theory to the OWEL setting.

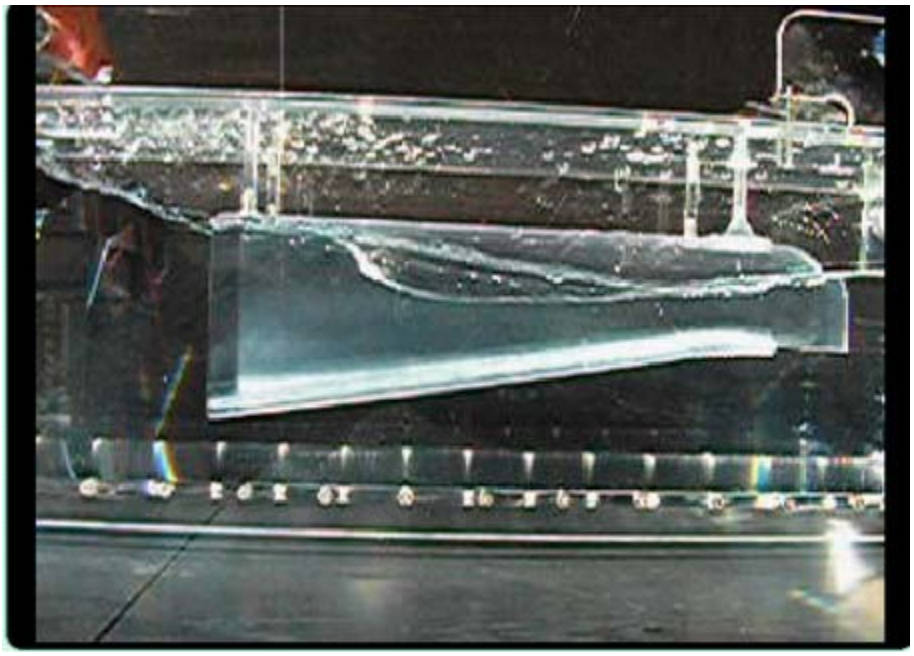

Introduction

The classical gravity current involves the flow of one fluid within another caused by density difference between the fluids. They have been a major area of study in fluid mechanics motivated by turbidity currents, saline intrusions, and atmospheric fronts. A review of work up to 1982 is given in the review article of Simpson [32]. The gravity current model of greatest interest here is where the upper fluid is air and a bubble of air is driven into quiescent or moving fluid (e.g. Gardner & Crow [17], Zukowski [34], Wilkinson [33], Keller & Chyou[24], Atrabi, Hosoda & Tada [10]). The moving bubble as gravity current is almost exactly the reverse problem in the OWEL wave energy convertor where the bubble is driven by the fluid.

Background on the OWEL WEC

Research and Development on the OWEL WEC has been underway for over ten years by teams at Offshore Wave Energy Ltd and IT Power Ltd in Bristol, with funding from DTI, EPSRC, SWRDA, and industrial funding [3]. Extensive experiments (Southampton, Plymouth, HMRC in Ireland) have been performed and analyzed, and the commercial CFD program ANSYS CFX has been used to simulate both 2D and 3D wave dynamics in a model duct. Agreement between computation and experiment has been reasonable, but only the simplest configurations have been tested (e.g. Leybourne et al. [26]).

The Surrey group has been working on modelling the OWEL WEC beginning with the Surrey Sloshing Initiative [2]. Most recently, the group has been working on an EPSRC-funded three year project whose aim is to provide the underpinning mathematics for the modelling of the OWEL WEC [1]. That project, which runs to 2016, has the principal aims of (a) developing fast and robust algorithms for a shallow water model for the interior fluid motion in the vessel, (b) include the dynamic coupling between fluid motion and vessel motion, (c) identify the resonance structure of the components (vessel, interior fluid, exterior fluid, mooring, etc) and their interaction.

The next generation research direction is effective modelling of the power take off (PTO). Capturing the PTO requires accurate modelling of the two-phase flow induced by the incoming wave and trapped moving bubble of air. The strategy is to model this two-phase flow using the theory of gravity currents.

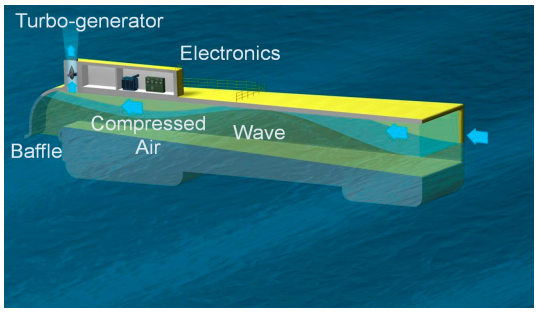

Figure 1: Schematic of the OWEL wave energy converter [3].

Gravity currents with air pocket

The first experimental studies on non-Boussinesq gravity currents were on air-cavity motion in horizontal ducts by Zukoski [34] (Z), Gardner and Crow [17] (GC) and Wilkinson [33] (W) to determine the front speeds and shapes of the air cavities. In all these experiments, air-cavity fronts were produced by opening, fully or partially, one end of a closed duct filled with water. Benjamin [12] (B) derived a theory for the steady propagation of such air-cavities in a rectangular channel, neglecting the effects of surface tension and viscosity at the solid boundaries and assuming that the flow upstream and downstream of the front was hydrostatic and that within the current there was no relative flow. By writing down the bulk conservation of mass, momentum and energy in a control volume moving with the air-cavity front, Benjamin determined the front speed as a function of the downstream water depth h and the duct depth D and showed that the shape of the air-cavity profile for the energy-conserving flow is similar to the cavity profile shown in Figure 2(b) with the cavity depth asymptotically approaching $\frac{1}{2}D$ downstream of the front [11].

Figure 2 shows schematics of the flow field superimposed on a potential OWEL configuration. In the OWEL configuration the wave will come in from the right with the bubble moving to the left, and here that pattern is reversed to correspond to the gravity current experiments. When the flow is inviscid it is time reversible and so the correspondence is exact, and for dissipative flows the energy balance needs to be adjusted for the reverse flow.

Benjamin [12] also showed that physically possible flows exist only with $h \geq D$ and that energy is dissipated when $h > \frac{1}{2}D$ [11]. Benjamin suggested that when the water from the open end of the rectangular duct (with $d = D$) is throttled, as in the three experimental studies mentioned above, steady flows would probably exist only for $h/D \geq .65$ and air-cavities in such flows would be similar to the profile depicted in Figure 2(d) [11]. However, Wilkinson found experimentally that when the water depth at the duct outlet is $.5 < h/D \leq .78$ the flow would become unsteady but the cavity front has the shape of Benjamin's energy conserving cavity ($h = \frac{1}{2}D$) followed by a hydraulic jump as sketched in Figure 2(c) which travels at a speed slower than that of the cavity front [11]. Wilkinson also observed that the flow becomes steady when $h/D > .78$ at the water outlet with the air-cavity shape as shown in Figure 2(d).

Baines, Rottman and Simpson (1985) (BRS) conducted similar experiments for the instantaneous release of a constant volume of air into water in a long horizontal rectangular tube but with both ends closed. The volume of air is confined at one of the ends before it is released. They observed that the motion of the air-cavity after release may be divided into three phases. Over the first phase the cavity front is established within a few percent of a second after release, and very quickly accelerates up to a constant speed and travels at this speed before transition into the second phase. During the second phase, the front speed decreases monotonically. Finally, in the third phase, the cavity front executes a series of erratic stops and starts before coming entirely to rest [11]. The independent parameters in the experiments, are the initial cavity length X_0 and the initial depth h_0 of the water

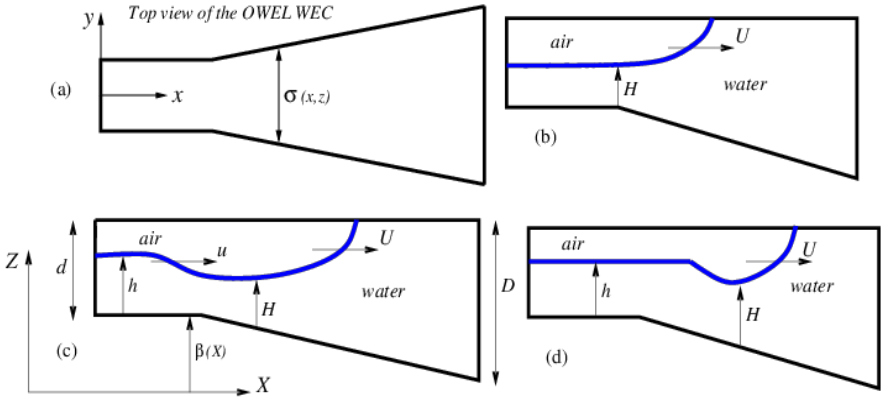

Figure 2: The three possible types of air-cavity profiles inside an OWEL-type vessel, with the flow direction reversed to correspond to the gravity current experiments. (a) OWEL cross-section. (b) Smooth steady air-cavity profile. (c) A smooth cavity front with a downstream hydraulic jump. (d) A steady cavity with a gravity-current type front.

under the cavity. The air-cavity properties are a function of the independent parameters. BRS observed that for $0 \leq h_0/D \leq .3$ over the first phase, the cavity front evolves into Benjamin's energy-conserving shape (Figure 2(b)) and simultaneously, the water displaced by the advancing cavity rushes in the opposite direction in the form of a surge. When the surge reaches the tube end it is reflected as a hydraulic jump [11] and the cavity has the shape shown in Figure 2(c) similar to what was observed by Wilkinson. But in the experiments and theory developed by BRS the jump has a slightly greater speed than that of the cavity front which is different from Wilkinson's observations for the propagation of the hydraulic jump for a tube with one end open. The hydraulic jump eventually overtakes the cavity front which has maintained constant shape and speed and abruptly reducing its speed and depth (Figure 2 (d)). BRS also discussed the shape and speed of the cavity front for other ratios of h_0/D. By applying Benjamin's theory and including the corrected surface tension effects first suggested by Wilkinson, and the classical theory of hydraulic jumps, BRS developed a theory for the front speed and shape of the cavity as a function of time after release. Following the work of B, GC, W and BRS the strategy going forward in modelling the motion of air-cavity fronts inside an OWEL-type vessel is as follows:

- Build a physical model of the OWEL wave energy converter with both ends closed, based on the specifications provided by the engineering team at Offshore Wave Energy Ltd and IT Power.
- Conduct a series of model tests to experimentally record the motion of *constant-volume* air cavities inside the OWEL model. To contain a constant volume of air a vertical gate would be installed inside the model at a distance X_0 from one end. To start the experiments the gate would be withdrawn in a fraction of a second releasing the air into the duct. The experiments can be done for different values of h_0/D or h_0/d and can be repeated for different values of X_0

from each end of the model. The purpose of these experiments is to determine the front speed and shape of the cavity as a function of time after release. The experimental results can be compared to previous results on the motion of air-cavities in tubes with constant rectangular cross-section. The three possible shapes of air-cavities inside the OWEL model are sketched in Figure 2. The model tests can be conducted in EnFlo at the University of Surrey [4].

- Develop a theory for the flow of constant volume air cavities in an OWEL-type vessel (with both ends closed) by extending Benjamin's theory on gravity currents and using the classical theory of hydraulic jumps for ducts with variable cross-section.

- Extension of the f-wave high-resolution finite volume methods of [5] for the two-layer non-Boussinesq shallow-water equations with OWEL-type geometry to model wetting-drying of the rigid-lid. The strategy is to use the speed and height of the cavity front from the background theory as the speed and height of the wet-dry front in the numerical model. And use the shock and rarefaction wave theory of [5] to model the interfacial wave numerically.

- After validating the OWEL air-cavity theory and the f-wave finite volume solvers we would be in a position to propose an optimal geometry for the OWEL WEC which results in the "best speed" for the cavity front as a function of the input wave (and other parameters). The speed of the front plays an important role in the performance of the PTO.

Improved influx-efflux boundary conditions

The above proposed experiments and theory are for a closed system, whereas the OWEL WEC has influx and efflux boundary conditions. The above experiments and theory can be modified to take into account these boundary conditions.

Experimentally, one can close the water inlets/outlets and the air outlet, and release a pocket of air into the duct by withdrawing the gates as sketched in Figure 3(a) and (c). Then when the air-cavities are established the water inlets and outlets and the air outlet would be opened so that we will have full control of the water flow rates and the air flow rate by measuring its pressure at the outlet using a pressure gauge. By adjusting the mass flow rates we would be able to push the cavity front to the end of the model where the pressure gauge or the PTO system is placed. The experiments can be repeated for different values of h_0/D and X_0 and with different amounts of the mass flowrates. The purpose of these experiments is to determine the front speed, shape of the cavity and pressure of the moving air pocket at the PTO system as a function of time after the air-cavity is established with different influx-efflux boundary conditions.

A theory for the flow of air cavities inside the model of the OWEL with influx-efflux boundary conditions and PTO system can be developed by extending the theory of B, GC, W, BRS and KC on air-cavity gravity currents and using the classical theory of hydraulic jumps for ducts with variable cross-section. Theory and experiments can be compared for validation.

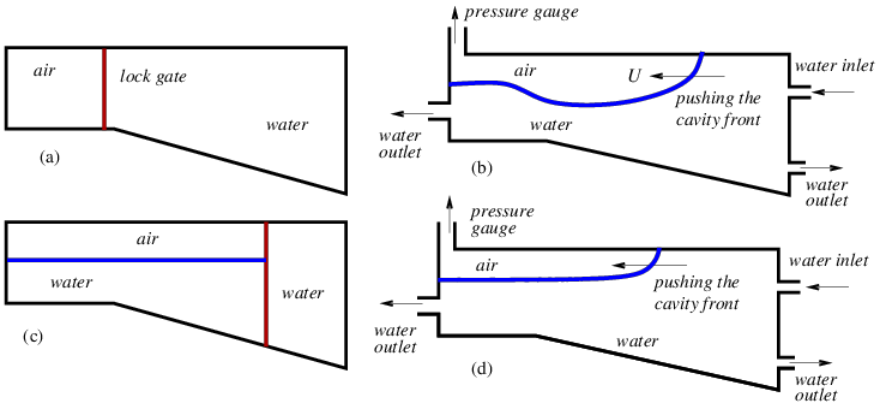

Figure 3: Two possible scenarios for producing air-cavities inside a model of the OWEL WEC with influx-efflux boundary conditions with pushing the cavity front to the PTO system.

Gravity currents and lock-exchange theories

Gravity currents produced by lock-exchange experiments also provide fundamental information about the speed of gravity currents. The gravity current and non-Boussinesq lock-exchange theories and experiments for two layer fluid flows inside rectangular channels with a rigid-lid are studied in [12, 30, 24, 31, 28, 27] and references therein, where usually a fluid of density ρ_1 is separated by a vertical barrier at the mid-point of the channel from fluid of density ρ_2, with $\rho_2 < \rho_1$. By rapidly removing the lock gate the flow is started in such a way that the heavy fluid intrudes into the expanse of lighter fluid.

Shin, Dalziel and Linden [31] (SDL) presented new theory and experiments, on gravity currents produced by a lock exchange, which suggest that dissipation is unimportant when the Reynolds number is sufficiently high. Their theory resulted in a new front Froude number in a deep ambient. Lowe, Rottman and Linden [27] (LRL) described the results of an experimental study on the non-Boussinesq lock-exchange problem. They developed a two-layer hydraulic theory to model the experiments. Their theory assumes that a light gravity current propagates along the top of the channel and a heavy gravity current propagates along the bottom of the channel in the opposite direction. The two wet-dry fronts are assumed to be connected by either a combination of an internal bore and an expansion wave when $\gamma^\star < \gamma \leq 1$, or just an expansion wave when $0 < \gamma \leq \gamma^\star$ where γ is the density ratio and $\gamma^\star$ is a critical density ratio. They also discovered that the connection of the light and heavy gravity currents by a rarefaction wave can be applied to the full range of γ.

Adapting and modifying the work of SDL and LRL to the OWEL configuration, a potential study is as follows. Conduct experimental tests for the Boussinesq and non-Boussinesq lock-exchange problem (with two different liquids) for the OWEL model (with both ends closed) to record the motion of light and heavy gravity currents over variable cross-section and measure the speed and height of the currents as a function of time after release. Extending the two-layer hydraulic theory of RLR to develop a

new theory for the gravity currents over variable cross-section. The extended theory would be validated against the experiments. The both light and heavy gravity current front speeds and heights would be used in the f-wave finite volume solvers to numerically simulate the Boussinesq and non-Boussinesq lock-exchange problems.

Review of the Keller-Chyou experiments

Keller and Chyou [24] (KC) studied the hydraulic lock-exchange theory experimentally and analytically for the problem of emptying a horizontal water-filled rectangular channel by means of pressurized air. Depending on the volume flow of pressurized air they suggested different possible flow regimes for the propagation of the wet-dry fronts along the top and bottom of the channel. The flow regimes that are relevant for the OWEL project are sketched in Figure 4. The inlet for the air to enter the duct is a small tube connected to the upper part of the channel to prevent a counter running gravity current of water to the air reservoir. On the other hand, the outlet for the water to leave the channel is smaller than the channel height in order to provide a throttling effect to establish a front travelling at constant speed. The speed of the air-cavity front can be adjusted by either the over pressure in the reservoir or the opening of the outlet. With different combinations of air pressure and outlet dimension, different flow regimes are observed in a rectangular channel as shown in Figure 4.

Using Benjamin's theory and a two-layer hydraulic theory, KC developed a new theory for the motion of air-cavities resulting from blowing of air into a water-filled channel. The theory of Armi (1986) for the rarefaction waves is corrected in KC's theory. As discussed in [24] small volume flow rates of pressurized air $0 < Q < .2806$ result in dissipative gravity currents moving at subcritical speed with respect to the flows behind them. The cavity profile for this flow regime is sketched in Figure 4(c). Increasing the volume flow beyond a certain limit $.1404 < Q < .5$ leads to a non-dissipative gravity current which moves at the Froude number $\sqrt{2}$ and is followed by a hydraulic jump as sketched in Figure 4(b). Details of the bifurcation of the solutions where the domains of validity of these two flow regimes overlap is discussed in [23]. Increasing the volume flow rate further $.5 \leq Q \leq \sqrt{2} + .5$ leads to a non-dissipative air-cavity which moves at the Froude number $\sqrt{2}$ and is followed by a rarefaction wave as sketched in Figure 4(d).

Adapting and modifying the approach of KC to the OWEL configuration, we propose the following studies. Modify the KC experiments to the OWEL configuration, and conduct model tests at EnFlo for the problem of emptying the water-filled OWEL by means of pressurized air, a schematic of which is shown in Figure 4. The purpose of these experiments is to determine the front speed and shape of the air-cavity as a function of time for different combinations of air pressure and outlet dimension. Three possible flow regimes are sketched in Figure 4. A series of Froude numbers at different sections of the model can be expressed as functions of the dimensionless height and dimensionless volume flow rate similar to that proposed by KC. An analogous theory can be developed and the experimental results can be compared to see how the variable cross-section of the OWEL could change the Froude numbers, shape of the air-cavity, and the volume flow rate.

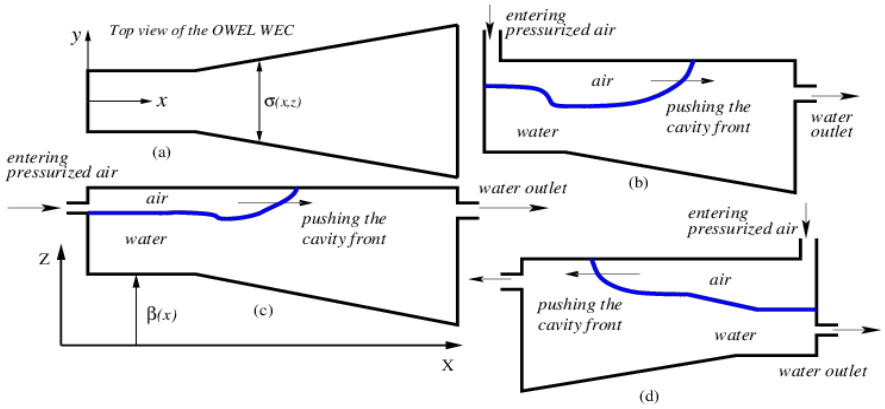

Figure 4: Emptying OWEL by means of pressurized air and the possible flow regimes. (a) OWEL cross-section. (b) Loss-free air cavity followed by a hydraulic jump. (c) Dissipative air-cavity. (d) Loss-free air-cavity followed by a rarefaction wave.

It is proposed to develop a new theory for the problem of emptying the water-filled OWEL by means of pressurized air by extending the theory of KC which is for ducts with constant rectangular cross-section. Theoretical results can be compared with the experimental results. After validating the theory we will be able to optimise the geometry of the OWEL WEC to determine maximum flow rates with constant inlet and outlet flow.

Direct numerical simulation of gravity currents

Härtel, Kleiser, Michaud and Stein [21] (HKMS) used a direct numerical simulation (DNS) approach to study the gravity currents numerically in a plane channel. The numerical method, that is employed for the problem of lock-exchange flow between two gases in the Boussinesq limit, is based on a mixed spectral and spectral-element discretization in space together with finite differences in time [21]. The schematic of the configuration of interest is shown in Figure 5 where two gases are initially separated by a vertical membrane. After the removal of the membrane, a heavy-gas front and a light-gas front develop and propagate along the lower and the upper channel wall, respectively [21]. HKMS used the Boussinesq equations in which density differences are assumed to be small. The dimensionless governing equations are [18, 21]

$$\left.\begin{aligned} &\frac{\partial u_k}{\partial x_k} = 0\,, \\ &\frac{\partial u_i}{\partial t} + \frac{\partial\,(u_k u_i)}{\partial x_k} = -\frac{\partial p}{\partial x_i} + \frac{1}{\sqrt{Gr}}\frac{\partial^2 u_i}{\partial x_k \partial x_k} + T\delta_{i3}\,, \\ &\frac{\partial T}{\partial t} + \frac{\partial\,(T u_k)}{\partial x_k} = \frac{1}{\sqrt{GrPr^2}}\frac{\partial^2 T}{\partial x_k \partial x_k}\,, \end{aligned}\right\} \tag{1}$$

where u_i denotes the velocity components, p the pressure and T the temperature. The variations in density are assumed to be caused by variations in temperature

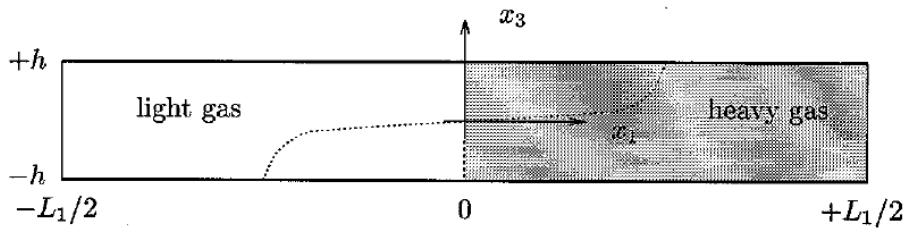

Figure 5: Schematic of lock-exchange flow between two gases in a channel of length L_1 and height $2h$. This is Figure 1 in [21].

such that [21]

$$\frac{\widetilde{\rho} - \widetilde{\rho}_0}{\widetilde{\rho}_0} = \beta \left(\widetilde{T} - \widetilde{T}_0 \right) , \tag{2}$$

where $\widetilde{\rho}_0$ and $\widetilde{T}_0$ are the reference values of density and temperature, respectively, and β is the heat expansion coefficient of the fluid. The flow variables in (2) with tildes are dimensional. The governing equations in (1) are nondimensionalized by the channel half-width, h, the temperature difference, $\Delta\widetilde{T} = \widetilde{T}_{\max} - \widetilde{T}_{\min}$, and the buoyancy velocity, $\widetilde{u}_b$, [21]

$$\widetilde{u}_b = \sqrt{g'h} \, ,$$

where g' is the reduced gravity $g' = g\beta\Delta\widetilde{T}$. The pressure is normalized by $\widetilde{\rho}\widetilde{u}_b^2$ and the dimensionless temperature is

$$T = \frac{\widetilde{T} - \widetilde{T}_{\min}}{\Delta T} \, .$$

In equation (1) Pr is the Prandtl number

$$Pr = \frac{\nu}{\kappa} \, ,$$

which is the ratio of kinematic viscosity ν and molecular diffusivity of temperature κ, and Gr is the Grashof number [18]

$$Gr = \left(\frac{\widetilde{u}_b h}{\nu} \right)^2 \, .$$

HKMS used an extension of the numerical method of [19], which was developed for the simulation of transition and turbulence in plane channel flow, to solve the governing equations (1) numerically. Time-dependent terms are discretized by a semi-implicit finite-difference scheme, and the diffusive and the buoyancy terms are discretized using the second-order Crank-Nicolson scheme while a third-order low-storage Runge-Kutta method is used for the nonlinear terms [21]. The boundary conditions for the lock-exchange problem are the frictionless end walls where the flow is assumed to possess a mirror symmetry with respect to $x_1 = \pm L_1/2$ and $x_2 = \pm L_2/2$. The top and bottom boundaries at $x_3 = \pm h$ are either rigid no-slip walls or no-stress (free-slip) boundaries, and they can be either isothermal or adiabatic [21]. To validate their code, simulations of Rayleigh-Bénard convection are

performed with periodic boundary conditions at $x_{1,2} = \pm L_{1,2}/2$ and compared with theoretical predictions and reference data from literature. The assumption of symmetry or periodicity in the longitudinal (x_1) and lateral (x_2) directions allows for the application of a Fourier spectral discretization in the x_1 and x_2 directions where the dependent variables in the finite-differences can be expanded in a complex Fourier series. These expansions simplify to expansions of the flow variables in real sine and cosine series with symmetric boundary conditions at the rigid-walls which reduce the computational costs significantly. The discretization of the resulting equations in the wall-normal direction x_3 is accomplished by a spectral element method. See [21] for the details of the discretizations. Using this method, the simulations of two-dimensional lock-exchange flows revealed the typical characteristics of intrusion fronts which were observed in experimental studies [21]. Numerical experiments are performed for different Grashof numbers. Among them are the formation of a pronounced head of the front, with a foremost point being raised above the wall, and strong Kelvin-Helmholtz billows which develop at the interface between the light and heavy fluid [21]. The instability of the interface, however, is not observed for small Grashof numbers in the numerical experiments of HKMS. By a systematic variation of the Grashof number the influence of viscous diffusion on the characteristics of the propagating fronts is assessed as is shown in Figure 7 in [21].

Direct numerical simulations are performed of gravity-current fronts in the lock-exchange configuration by Härtel, Meiburg and Necker [22] (HMN). The governing equations are the Boussinesq equations which neglect variations in density $\widetilde{\rho}$ except for the buoyancy term of the momentum equation (a tilde denotes a dimensional variable) and in nondimensional form using the notation of [22] are

$$\left.\begin{aligned} &\frac{\partial u_k}{\partial x_k} = 0\,, \\ &\frac{\partial u_i}{\partial t} + \frac{\partial\,(u_k u_i)}{\partial x_k} = -\frac{\partial p}{\partial x_i} + \frac{1}{\sqrt{Gr}}\frac{\partial^2 u_i}{\partial x_k \partial x_k} + \rho e_i^g\,, \\ &\frac{\partial \rho}{\partial t} + \frac{\partial\,(\rho u_k)}{\partial x_k} = \frac{1}{\sqrt{GrSc^2}}\frac{\partial^2 \rho}{\partial x_k \partial x_k}\,, \end{aligned}\right\} \tag{3}$$

where $e_i^g = (0, 0, -1)$ is the unit vector in the direction of gravity acceleration. The equations are nondimensionalized by the channel half-height $\widetilde{h}$, the average density $\widetilde{\rho}_a$, and the buoyancy velocity $\widetilde{u}_b = \sqrt{\widetilde{g}'\widetilde{h}}$ with $\widetilde{g}' = \widetilde{g}\dfrac{\Delta\widetilde{\rho}}{\widetilde{\rho}_a}$ where $\Delta\widetilde{\rho} = \widetilde{\rho}_{\max} - \widetilde{\rho}_{\min}$ is the difference between the reservoir densities of light and heavy fluid, respectively [22]. The nondimensional pressure p and density ρ are

$$p = \frac{\widetilde{p}}{\widetilde{\rho}_a \widetilde{u}_b^2} \quad \text{and} \quad \rho = \frac{\widetilde{\rho} - \widetilde{\rho}_{\min}}{\Delta\widetilde{\rho}}\,,$$

and the two dimensionless numbers in (3) are the Grashof number $Gr = \left(\dfrac{\widetilde{u}_b \widetilde{h}}{\widetilde{\nu}}\right)^2$ and the Schmidt number $Sc = \dfrac{\widetilde{\nu}}{\widetilde{K}}$ where $\widetilde{K}$ is the molecular diffusivity in the density field. If the differences in density are caused by differences in temperature, the Schmidt number is identical to the Prandtl number and the convection-diffusion

equation for the density variation in (3) becomes the thermal energy equation in (1) [22]. The Boussinesq equations (3) can be converted to a vorticity-streamfunction formulation for strictly two-dimensional flows. Denoting the streamfunction by ψ and the vorticity by ω the governing equations become [22]

$$\left.\begin{aligned} &\frac{\partial \omega}{\partial t} + u_k \frac{\partial \omega}{\partial x_k} = \frac{1}{\sqrt{Gr}} \frac{\partial^2 \omega}{\partial x_k \partial x_k} - \frac{\partial \rho}{\partial x_1}\,, \\ &\frac{\partial^2 \psi}{\partial x_k \partial x_k} = -\omega\,, \\ &\frac{\partial \rho}{\partial t} + \frac{\partial\,(\rho u_k)}{\partial x_k} = \frac{1}{\sqrt{GrSc^2}} \frac{\partial^2 \rho}{\partial x_k \partial x_k}\,, \end{aligned}\right\} \tag{4}$$

where

$$\omega = \frac{\partial u_3}{\partial x_1} - \frac{\partial u_1}{\partial x_3}\,, \quad u_1 = \frac{\partial \psi}{\partial x_3}\,, \quad u_3 = -\frac{\partial \psi}{\partial x_1}\,.$$

For the simulations, high-order numerical methods are used, based on spectral and spectral-element discretizations and compact finite differences of [21] which uses the velocity-pressure formulation (3). A spectral-element collocation technique is used for the spatial discretizations in the wall-normal direction x_3, and Fourier expansions are used in the longitudinal and lateral directions. For time discretization, a semi-implicit method is employed which along with the spectral-element discretization, provides good flexibility of the numerical mesh in the normal direction [22]. For simulations at very high Grashof numbers, another existing highly optimized code for the simulation of two-dimensional particle-driven flows is adopted [22] which is based on the vorticity-streamfunction formulation (4). This code employs equidistant grids in both directions with an explicit third-order accurate low-storage Runge-Kutta method for integration in time, along with a spectral method in the longitudinal direction [22]. The boundary conditions at $x_3 = \pm 1$ are either rigid no-slip walls or slip boundaries. See [22] for a detailed discussion of the numerical method. The main objective of the numerical study of two and three- dimensional lock-exchange flows by HMN was a detailed analysis of the flow structure at the foremost part of the gravity-current front. The three-dismensional simulation of HMN for a front spreading along a no-slip boundary at a Reynolds number of about 750 reveals all the features that obseved in the experimental results near the front, including the lobe-and-cleft structure of the front leading edge [22]. Results show that the foremost point is not a stagnation point in a translating system in contrast with the previous theoretical assumptions about the nose of the front. The stagnation point is located below and slightly behind the foremost point in the vicinity of the wall [22]. For high Reynolds number simulations the two-dimensional particle-driven code is used for both no-slip and slip boundaries. It is observed that no qualitative changes in the flow structure at the head occur at high Reynolds numbers [22]. A linear-stability analysis of the flow at the head of two-dimensional gravity-current fronts is presented in [20] to clarify the instability mechanism that leads to the formation of the complex lobe-and-cleft pattern which is commonly observed at the leading edge of gravity currents propagating along solid boundaries [20]. Necker, Härtel, Kleiser and Meiburg [29] (NHKM) presented high-resolution simulations of particle-driven gravity currents in the lock-exchange configuration. Their study concentrated on dilute flows with small density differences between particle-laden and clear fluid.

For the mathematical description of the particulate phase an Eulerian approach is used with a transport equation for the local particle-number density. The governing equations are integrated with the numerical scheme of HKMS and HMN.

Birman, Martin and Meiburg [13] (BMM) and Birman and Meiburg [14] (BM) employed a high-resolution numerical method to simulate Boussinesq and non-Boussinesq gravity currents in the lock-exchange configuration over horizontal and sloping bottom geometries. BMM and BM used the following nondimensional equations for their direct numerical simulation of the non-Boussinesq gravity currents

$$\left.\begin{aligned} &\nabla \cdot \mathbf{u} = 0\,, \\ &\rho \frac{D\mathbf{u}}{Dt} = \frac{1}{1-\gamma}\rho \mathbf{e}_g - \nabla p + \frac{1}{Re}\nabla \cdot (2\rho \mathbf{S})\,, \\ &\frac{D\rho}{Dt} = \frac{1}{Pe}\nabla^2 \rho\,, \end{aligned}\right\} \tag{5}$$

with $\rho = \rho_2 + c\,(\rho_1 - \rho_2)$ where the density of the heavy and light fluids are denoted by ρ_1 and ρ_2, respectively. The third equation in (5) is a convection-diffusion equation for the concentration c of the heavier fluid. $\mathbf{e}_g$ is the unit vector, $Re = \dfrac{u_b H}{\nu}$ is the Reynolds number with the channel height H, kinematic viscosity ν, and the buoyancy velocity $u_b = \sqrt{g' H}$ where the reduced gravity $g' = g\,(1-\gamma)$ and $\gamma = \rho_2/\rho_1 < 1$, and $Pe = \dfrac{u_b H}{K}$ is the Péclet number with the molecular diffusivity K. Reynolds and Péclet numbers are related by the Schmidt number $Sc = \dfrac{\nu}{K}$ which is the ratio of kinematic viscosity to molecular diffusivity, so that $Pe = ReSc$. In (5) $\mathbf{S}$ is the rate of strain tensor, p the pressure, $\mathbf{u} = (u, v)^T$ indicates the velocity vector, and D/Dt denotes the material derivative of a quantity. For the purpose of direct numerical simulations, the governing equations are recast into the vorticity-streamfunction formulation [13, 14]

$$\left.\begin{aligned} &\nabla^2 \psi = -\omega\,, \\ &\frac{D\omega}{Dt} = \frac{1}{Re}\nabla^2 \omega - \frac{\rho_x}{(1-\gamma)\,\rho} + \frac{\rho_z}{\rho}\frac{Du}{Dt} - \frac{\rho_x}{\rho}\frac{Dv}{Dt} \\ &\qquad\qquad + \frac{1}{\rho Re}\left(2\rho_x \nabla^2 v - 2\rho_z \nabla^2 u + 4\rho_{xz} v_z + (u_z + v_x)\,(\rho_{xx} - \rho_{zz})\right)\,, \end{aligned}\right\} \tag{6}$$

where ψ is the streamfunction, $\omega = v_x - u_y$ the vorticity in the spanwise direction, $u = \partial\psi/\partial y$, and $v = -\partial\psi/\partial z$. BMM and BM considered rectangular domains of length 32 for their simulations. Initially, slip conditions are enforced along all of the walls. Consequently, $\psi = 0$ and $\omega = 0$ is assigned along all boundaries [13]. The concentration satisfies Neumann boundary conditions along all walls, in order to enforce zero diffusive mass flux [13]. The effect of no-slip boundary conditions along the top and bottom boundaries is evaluated by taking $\psi = 0$ and $\omega = -\partial^2\psi/\partial z^2$ [13]. For the numerical simulations, equidistant grids are employed in the rectangular computational domain. Spectral Galerkin methods are used in representing the streamwise dependence of the streamfunction and the vorticity fields [13, 14]. Vertical derivatives are approximated on the basis of the compact finite-difference stencils of [25]. As in the Boussinesq investigation of HMN, derivatives of the density field are computed from compact finite differences in both directions [13, 14].

At interior points, sixth-order spatially accurate stencils are used, with third- and fourth-order accurate stencils employed at the boundaries [13, 14]. The flow field is advanced in time by means of the third-order Runge-Kutta scheme described by HMN [13, 14]. The material derivatives of the velocity components appearing in the vorticity equation in (6) are rewritten in terms of the local time derivative plus the convective terms and the spatial derivatives of the convective terms are evaluated in the usual high-order way [13, 14]. The local time derivative is computed by a backward extrapolation which is consistently used during the successive Runge-Kutta substeps [13, 14]. The Poisson equation for the streamfunction in (6) is solved once per time step in Fourier space. See the papers by BMM and BM for more details. The non-Boussinesq simulations of gravity currents for density ratios of $\gamma = .92$, $\gamma = .7$ and $\gamma = .2$ are presented by BMM and BM and discussed.

Our strategy going forward for the OWEL project could be:

- Adaptation of the DNS approach of HKMS and HMN to simulate the Boussinesq gravity current inside a vessel with the OWEL geometry and validate the Boussinesq DNS code against the theory and experiments.
- Adaptation of the DNS approach of BMM and BM to simulate the non-Boussinesq air-cavity gravity current inside a vessel with the OWEL geometry and validate the non-Boussinesq DNS code against the theory and experiments.

Finite volume method for air-cavity gravity current with compressibility effects

A possible scenario for the numerical simulations of fluid flows inside the OWEL wave energy converter in order to study the effects of compressibility on the PTO system is to employ a relatively simple two-fluid model to simulate the non-Boussinesq air-cavity gravity current. For this purpose air-water mixture can be assumed to behave as a homogeneous inviscid compressible fluid. Air and water share, locally, the same pressure, temperature and velocity. Conservation of mass (1 per fluid), balance of linear momentum and total energy are [15]

$$\left.\begin{aligned}
\frac{\partial(\alpha_l\rho_l)}{\partial t}+\frac{\partial(\alpha_l\rho_l u)}{\partial x}+\frac{\partial(\alpha_l\rho_l v)}{\partial y}+\frac{\partial(\alpha_l\rho_l w)}{\partial z} &= 0\,,\\
\frac{\partial(\alpha_g\rho_g)}{\partial t}+\frac{\partial(\alpha_g\rho_g u)}{\partial x}+\frac{\partial(\alpha_g\rho_g v)}{\partial y}+\frac{\partial(\alpha_g\rho_g w)}{\partial z} &= 0\,,\\
\rho\left(\frac{\partial u}{\partial t}+u\frac{\partial u}{\partial x}+v\frac{\partial u}{\partial y}+w\frac{\partial u}{\partial z}\right)+\frac{\partial p}{\partial x} &= 0\,,\\
\rho\left(\frac{\partial v}{\partial t}+u\frac{\partial v}{\partial x}+v\frac{\partial v}{\partial y}+w\frac{\partial v}{\partial z}\right)+\frac{\partial p}{\partial y} &= 0\,,\\
\rho\left(\frac{\partial w}{\partial t}+u\frac{\partial w}{\partial x}+v\frac{\partial w}{\partial y}+w\frac{\partial w}{\partial z}\right)+\frac{\partial p}{\partial z} &= -\rho g\,,\\
\frac{\partial(\rho E)}{\partial t}+\frac{\partial(\rho H u)}{\partial x}+\frac{\partial(\rho H v)}{\partial y}+\frac{\partial(\rho H w)}{\partial z} &= -\rho g w\,,
\end{aligned}\right\} \qquad \text{(a)}$$

where subscripts (l, g) denote liquid and gas, respectively. Hence α_l and α_g denote the volume fraction of liquid and gas, respectively, and satisfy $\alpha_l + \alpha_g = 1$. The

total density, specific total energy and specific total enthalpy are, respectively

$$\left.\begin{aligned} \rho &:= \alpha_l\rho_l + \alpha_g\rho_g\,, \\ E &= e + \tfrac{1}{2}\left(u^2+v^2+w^2\right)\,, \\ H &:= E + \frac{p}{\rho}\,, \end{aligned}\right\}$$

where e is the specific internal energy. In order to close the system of partial differential equations (a), it is assumed that the pressure p is given as a function of parameters, $\alpha := \alpha_l - \alpha_g$, ρ and e

$$p = \mathscr{P}\left(\alpha, \rho, e\right) = \left(\gamma(\alpha) - 1\right)\rho e - \pi(\alpha)\,. \tag{b}$$

This is the extended equation of state which obeys the stiffened gas law. Once the two independent equations of state $p = \mathscr{P}_{l,g}(\rho_{l,g}, e_{l,g})$ are known, the extended equation of state (b) can be determined [15, 16]. The boundary conditions are the no-slip boundary conditions at the rigid boundaries. The two-fluid equations (a) are used for a scaling analysis for the interactions between aerated waves and the oyster wave energy converter in [8]. Dias, Dutykh and Ghidaglia [15] (ddg) used a second-order finite volume method to solve the two-fluid equations (a).

Our strategy going forward for the OWEL project could be:

- Adaptation of the finite volume approach of ddg for the two-fluid model (a) to simulate the inviscid compressible air-cavity gravity current inside the OWEL wave energy converter.
- Investigate the effects of compressibility on the PTO system with influx-efflux boundary conditions.

References

[1] http://personal.maths.surrey.ac.uk/st/T.Bridges/OWEL/

[2] http://personal.maths.surrey.ac.uk/st/T.Bridges/SLOSH/

[3] http://www.owel.co.uk/

[4] http://www.surrey.ac.uk/mes/research/aef/enflo/

[5] H. Alemi Ardakani, T.J. Bridges & M.R. Turner. *Adaptation of f-wave finite volume methods to the two-layer shallow-water equations in a moving vessel with a rigid-lid*, Preprint (2014).

[6] H. Alemi Ardakani, T.J. Bridges & M.R. Turner. *Dynamic coupling between horizontal vessel motion and two-layer shallow-water sloshing*, Preprint (2014).

[7] H. Alemi Ardakani, T.J. Bridges & M.R. Turner. *Shallow-water sloshing in a moving vessel with variable cross-section and wetting-drying using an extension of George's well-balanced finite volume solver*, Preprint (2015).

[8] H. Alemi Ardakani & F. Dias. *On the scaling analysis for wave-oyster interactions*, Internal Report, University College Dublin (2011).

[9] L. Armi. *The hydraulics of two flowing layers with different densities*, Journal of Fluid Mechanics **163** 27–58 (1986).

[10] H.B. Atrabi, T. Hosoda, & A. Tada. *Simulation of air cavity advancing into a straight duct*, ASCE J. Hydraulic Eng. **04014068** 1–9 (2015).

[11] W.D. Baines, J.W. Rottman & J.E. Simpson. *The motion of constant-volume air cavities in long horizontal tubes*, J. Fluid Mech. **161** 313–327 (1985).

[12] T.B. Benjamin. *Gravity currents and related phenomena*. J. Fluid Mech. **31** 209–248 (1968).

[13] V.K. Birman, J.E. Martin & E. Meiburg. *The non-Boussinesq lock-exchange problem. Part 2. High-resolution simulations*, J. Fluid Mech **537** 125–144 (2005).

[14] V.K. Birman & E. Meiburg. *High-resolution simulations of gravity currents*, J. Braz. Soc. Mech. Sci. & Eng. **28** 169–173 (2006).

[15] F. Dias, D. Dutykh, J.-M. Ghidaglia. *A two-fluid model for violent aerated flows*, Computers & Fluids **39** 283–293 (2010).

[16] S. Faure & J.-M. Ghidaglia. *Violent flows in aqueous foams I: Physical and numerical models*, European Journal of Mechanics B/Fluids **30** 341–359 (2011).

[17] C.G. Gardner & I.G. Crow. *The motion of large air bubbles in horizontal channels*, J. Fluid Mech. **43** 247–255 (1970).

[18] B. Gebhart, Y. Jaluria, R.L. Mahajan & B. Sammakia. *Buoyancy-Induced Flows and Transport*, Hemisphere Publishing Corporation, New York (1979).

[19] N. Gilbert & L. Kleiser. *Turbulence model testing with the aid of direct numerical simulation results*, In Proc. of the 8th Symposium on Turbulent Shear Flows, Munich, September 9–11 (1991).

[20] C. Härtel, F. Carlsson & M. Thunblom. *Analysis and direct numerical simulation of the flow at a gravity-current head. Part 2. The lobe-and-cleft instability*, J. Fluid Mech. **418** 213–229 (2000).

[21] C. Härtel, L. Kleiser, M. Michaud & C.F. Stein. *A direct numerical simulation approach to the study of intrusion fronts*, J. Eng. Math. **32** 103–120 (1997).

[22] C. Härtel, E. Meiburg & F. Necker. *Analysis and direct numerical simulation of the flow at a gravity-current head. Part 1. Flow topology and front speed for slip and no-slip boundaries*, J. Fluid Mech. **418** 189–212 (2000).

[23] J.J. Keller, W. Egli & J. Exley. *Force- and loss-free transitions between flow states*, ZAMP **36** 854–889 (1985).

[24] J.J. Keller & Y.-P. Chyou. *On the hydraulic lock-exchange problem*, ZAMP **42** 874–909 (1991).

[25] S.K. Lele. *Compact finite difference schemes with spectral-like resolution*, J. Comput. Phys. **103** 16–42 (1992).

[26] M. Leybourne, W. Batten, A.S. Bahaj, N. Minns, & J. O'Nians. *Experimental and computational modelling of the OWEL wave energy converter*, Third Int. Conf. Ocean Energy, ICOE2010 (2010).

[27] R.J. Lowe, J.W. Rottman & P.F. Linden. *The non-Boussinesq lock-exchange problem. Part 1. Theory and experiments*, J. Fluid Mech. **537** 101–124 (2005).

[28] B.M. Marino, L.P. Thomas & P.F. Linden. *The front condition for gravity currents*, J. Fluid Mech. **536** 49–78 (2005).

[29] F. Necker, C. Härtel, L. Kleiser & E. Meiburg. *High-resolution simulations of particle-driven gravity currents*, International Journal of Multiphase Flow **28** 279–300 (2002).

[30] J.W. Rottman & J.E. Simpson. *Gravity currents produced by instantaneous releases of a heavy fluid in a rectangular channel*, J. Fluid Mech. **135** 95–110 (1983).

[31] J.O. Shin, S.B. Dalziel & P.F. Linden. *Gravity currents produced by lock exchange*, J. Fluid Mech. **521** 1–34 (2004).

[32] J.E. Simpson. *Gravity currents in the laboratory, atmosphere, and ocean*, Ann. Rev. Fluid Mech. **14** 213–234 (1982).

[33] D.L. Wilkinson. *Motion of air cavities in long horizontal ducts*, J. Fluid Mech. **118** 109–122 (1982).

[34] E.E. Zukoski. *Influence of viscosity, surface tension, and inclination angle on motion of long bubbles in closed tubes*, J. Fluid Mech. **25** 821–840 (1966).